

Tropospheric adjustment to increasing CO₂: its timescale and the role of land–sea contrast

Youichi Kamae · Masahiro Watanabe

Received: 30 July 2012 / Accepted: 1 October 2012
© The Author(s) 2012. This article is published with open access at Springerlink.com

Abstract Physical processes responsible for tropospheric adjustment to increasing carbon dioxide concentration are investigated using abrupt CO₂ quadrupling experiments of a general circulation model (GCM) called the model for interdisciplinary research on climate version 5 with several configurations including a coupled atmosphere–ocean GCM, atmospheric GCM, and aqua-planet model. A similar experiment was performed in weather forecast mode to explore timescales of the tropospheric adjustment. We found that the shortwave component of the cloud radiative effect (SWcld) reaches its equilibrium within 2 days of the abrupt CO₂ increase. The change in SWcld is positive, associated with reduced clouds in the lower troposphere due to warming and drying by instantaneous radiative forcing. A reduction in surface turbulent heat fluxes and increase of the near-surface stability result in shoaling of the marine boundary layer, which shifts the cloud layer downward. These changes are common to all experiments regardless of model configuration, indicating that the cloud adjustment is primarily independent of air–sea coupling and land–sea thermal contrast. The role of land in cloud adjustment is further examined by a series of idealized aqua-planet experiments, with a rectangular continent of varying width. Land surface warming from quadrupled CO₂ induces anomalous upward motion, which increases high cloud and associated negative SWcld over land. The geographic distribution of continents regulates the spatial pattern of the cloud adjustment. A larger continent produces more negative SWcld, which partly compensates for

a positive SWcld over the ocean. The land-induced negative adjustment is a factor but not necessary requirement for the tropospheric adjustment.

Keywords Tropospheric adjustment · Radiative forcing · Boundary layer · Cloud radiative effect · Transpose-AMIP · Aqua-planet experiment

1 Introduction

During recent decades, general circulation models (GCMs) have played a major role in studies on past, present and future climate change. Recent works reveal that it is important to investigate changes in radiative forcing and feedback to perturbation of external forcing for understanding climate sensitivity, defined by the global mean surface air temperature (SAT) change in response to doubling of atmospheric CO₂ concentration. It is well known that instantaneous CO₂ forcing can lead to rapid responses in the atmosphere (e.g., vertical profile of temperature, humidity, cloud and circulation) without changes in global mean SAT, and therefore they induce adjustments in top of the atmosphere (TOA) radiative balance. The processes in the troposphere are called tropospheric adjustment (Gregory and Webb 2008, hereafter GW08; Andrews and Forster 2008; Dong et al. 2009; Colman and McAvaney 2011). Because of the fast timescale, these processes are often included in CO₂ radiative forcing and are referred to as effective radiative forcing (Knutti and Hegerl 2008; Webb et al. 2012, hereafter WLG12). Slowdown of the hydrological cycle, i.e., precipitation and evaporation, is also an essential aspect of tropospheric adjustment (Mitchell et al. 1987; Allen and Ingram 2002; Lambert and Webb 2008; Andrews et al. 2009, 2010; Bala et al. 2010).

Y. Kamae (✉) · M. Watanabe
Atmosphere and Ocean Research Institute, University of Tokyo,
5-1-5 Kashiwanoha, Kashiwa, Chiba 277-8568, Japan
e-mail: kamae@aori.u-tokyo.ac.jp

Hansen et al. (2005) summarized methods that can be used to diagnose the CO₂ radiative forcing. One is to run atmospheric GCMs (AGCMs) with fixed sea surface temperature (SST) and sea ice but with different CO₂ concentrations (Hansen et al. 2002). The effective radiative forcing is estimated as the radiative perturbation at the TOA, which includes the effects of stratospheric and tropospheric adjustments. This “fixed-SST method” has been widely used because of its convenience and lesser computational burden (Hansen et al. 2005). Another method that has been widely used is a regression method proposed by Gregory et al. (2004). In this approach, a coupled atmosphere–ocean GCM (AOGCM) or AGCM coupled with a slab ocean is integrated with control and abruptly increased CO₂ settings. A linear regression of global mean anomalies (changes between the two experiments) of net TOA radiative fluxes on global mean SAT anomaly is computed. The y-axis intercept of the regression line indicates the effective radiative forcing, while the equilibrium climate sensitivity and feedback parameter are given by the x-axis intercept and slope of the regression line. The regression method is useful to diagnose and compare forcing, feedback and equilibrium climate sensitivity among AOGCMs, without running them over centuries. In frameworks of the Coupled Model Intercomparison Project (CMIP) and Cloud Feedback Model intercomparison Project (CFMIP), inter-model spread and robustness of estimated radiative forcing with the above two methods were examined quantitatively (GW08; Andrews et al. 2012a; WLG12). Andrews et al. (2012a) pointed out some differences in effective radiative forcings estimated using the fixed-SST and regression methods, probably owing to a non-linear response of TOA radiative balance in the AOGCM integrations (Gregory et al. 2004).

However, the nature of tropospheric cloud adjustment has not been clearly stated in previous studies. The effective radiative forcing, particularly shortwave (SW) component of the cloud radiative effect (CRE; defined by the difference between all-sky and clear-sky fluxes; Cess et al. 1990), associated with cloud adjustment is estimated by GCMs but has large uncertainty (GW08, Andrews et al. 2012a; WLG12). Several processes potentially important for changes in cloud adjustment and SW CRE (hereafter SWcld) have been suggested. Dong et al. (2009) showed a decreasing total cloud fraction and positive SWcld associated with tropospheric adjustment by using the atmosphere component of HadSM3. Colman and McAvaney (2011) revealed that the essential part of positive perturbation in SW cloud radiation in tropospheric adjustment is not associated with cloud optical properties, but cloud fraction with a version of the Australian Bureau of Meteorology Research Centre (BMRC) climate model. They also pointed out similarities in patterns of tropospheric warming, drying, and instantaneous radiative heating in

zonal-mean, height-latitude sections. Watanabe et al. (2011) and Wyant et al. (2012, hereafter W12) reported a positive SWcld and shoaling of the marine boundary layer in the subtropics as factors contributing to tropospheric adjustment in the Model for Interdisciplinary Research on Climate version 5 (MIROC5) and SP-CAM, respectively. It is needed to clarify changes in cloud, temperature, humidity and boundary layer as well as their effects on changes of CRE in the tropospheric adjustment.

One possible way to explore the mechanisms of tropospheric cloud adjustment is to examine transient processes evolving on different timescales following an abrupt CO₂ increase. Because tropospheric adjustment is considered as rapid as stratospheric adjustment, it is difficult to detect transient evolution and processes of the tropospheric adjustment using annual or monthly-mean data. After CO₂ forcing is imposed, the model atmosphere warms fastest in the first year. This means that the number of samples is very limited, which results in considerable uncertainty in estimation of the adjustment because they contain interannual variability. In addition, a single sensitivity test also contains seasonality in the response to CO₂ increase. Dong et al. (2009) examined fast responses to CO₂ doubling from six-member ensemble experiments with December and June initial conditions. They presented timescales in the development of land surface warming and changes in tropospheric thermodynamic structure. Wu et al. (2012) conducted a 10-member ensemble of CO₂ doubling experiments, with initial conditions in different years. They concluded that the troposphere warms in 1 month, but atmospheric circulation adjusts on a longer timescale. However, the above methods have some limitation for investigating transient evolutions on sub-monthly timescales, because the samples do not cover interannual and seasonal variations.

There is a possibility that some aspects of tropospheric adjustment are driven by rapid warming of the land surface. When atmospheric CO₂ is increased in the model, land–sea thermal contrast evolves rapidly because the land surface warms up much faster than the ocean. This land–sea warming contrast in response to CO₂ increase (Manabe et al. 1991; Sutton et al. 2007; Dommenges 2009; Boer 2011) slows down atmospheric circulation and the hydrological cycle (Andrews et al. 2009; Dong et al. 2009; Bala et al. 2010; Fasullo 2010; Andrews et al. 2011), and also modifies cloud amount and the CRE (Lambert et al. 2011, hereafter LWJ11; W12). In response to CO₂ increases, reduction in stomatal conductance acts as a “CO₂ physiological forcing” (Sellers et al. 1996; Dong et al. 2009; Doutriaux-Boucher et al. 2009; Boucher et al. 2009; Andrews et al. 2011, 2012b) that reinforces the land–sea thermal contrast and associated changes in atmospheric circulation and hydrological cycle. The change in dynamical motion affects the cloud profile and total fractions as

well as associated CRE in tropospheric adjustment (GW08; LWJ11; W12). However, in the previous works, it was not clarified whether the land–sea warming contrast is essential for tropospheric adjustment. Some kinds of idealized model experiments such as aqua-planet experiments may clarify the role of land and associated temperature contrast between land and ocean for the tropospheric adjustment to increasing CO₂.

In this study, we aim to clarify the physical mechanisms of tropospheric cloud adjustment focusing on two aspects: its timescale and land–sea thermal contrast. We conducted abrupt CO₂ quadrupling (4×CO₂) experiments in a single model, but with various model and experimental configurations (AOGCM, AGCM, aqua-planet model, weather forecast approaches; Sect. 2). Transient adjustment processes on fast timescales are first investigated by a large-member ensemble experiment with increased signal-to-noise ratio, and then idealized model experiments based on an aqua planet are performed to examine the role of the land surface warming on the tropospheric adjustment. Section 2 describes the model used and experimental settings, i.e., standard CMIP5 (Taylor et al. 2012)/CFMIP2 (Bony et al. 2011) experiments and idealized runs. Section 3 explores immediate, transient, and slower processes in tropospheric adjustment, with particular attention to cloud and associated radiative changes over the ocean. Section 4 focuses on the land effect on tropospheric adjustment by investigating tropospheric responses through a series of idealized models with different continent sizes. Section 5 presents concluding discussions, highlighting study results and their significance.

2 Model and experiments

2.1 MIROC5

The GCM used is MIROC5 (Watanabe et al. 2010) developed jointly at the Atmosphere and Ocean Research Institute (AORI), University of Tokyo, National Institute

for Environmental Studies (NIES), and Japan Agency for Marine-Earth Science and Technology (JAMSTEC). This is one of the models contributing to CMIP5 (Taylor et al. 2012) and the Intergovernmental Panel on Climate Change (IPCC) Fifth Assessment Report (AR5). The atmospheric component of MIROC5 has resolution T85 in the horizontal, with vertical 40 Eta (η) levels. The ocean component model has approximately 1° horizontal resolution, and 49 vertical levels with an additional bottom boundary layer. MIROC5 reproduces cloud and water vapor generally well but underestimates high cloud relative to the other CMIP5 models (Jiang et al. 2012). The equilibrium climate sensitivity to doubling CO₂ in MIROC5 is 2.6 K, which is 1 K lower than in the previous model version, MIROC3.2 (Hasumi and Emori 2004) because of a difference in SWcld feedback (Watanabe et al. 2010; Shiogama et al. 2012). Dependencies of SWcld feedback and climate sensitivity on the structure of MIROC models are detailed in Watanabe et al. (2012).

2.2 4×CO₂ experiments

The control and abrupt 4×CO₂ experiments conducted in this study are summarized in Table 1, which shows model types (AOGCM or AGCM), experiment names following CMIP5 protocol, and ensemble size. First, we analyzed results of the 4×CO₂ experiments using MIROC5 AOGCM (piControl and abrupt4xCO2). The large abrupt forcing as 4×CO₂ is not realistic but could construct a response to a transient increase in CO₂ (Good et al. 2011), implying a usefulness of the abrupt 4×CO₂ experiment for understanding the behavior of climate system. In addition to a single-member long-term integration, we performed 12-member ensemble experiments starting from initial states 1 month apart, i.e., from January 1st, February 1st, and so on, to remove seasonality. Second, fixed-SST experiments (amip and amip4xCO2; AMIP hereafter) were run for 30 years, from 1979 to 2008, to estimate effective radiative forcing. In addition, an aqua-planet experiment

Table 1 Summary of experimental configurations using MIROC5 analyzed in this study

	Type of model	CMIP5 label	Ensemble member	Temporal resolution	Length for calculating climatology
	AOGCM	piControl, abrupt4xCO2	12	1 day	–
	AMIP	amip, amip4xCO2	1	–	30 years
	Transpose-AMIP II (TAMIP)	–	64	3 h	–
Pairs of experiments (control and 4×CO ₂) were conducted in individual configurations. CMIP5 labels are according to Taylor et al. (2012)	Aqua-planet experiment (APE)	aquaControl, aqua4xCO2	1	–	5 years after 1 year spin-up
	L60, L120, L180, L240, L300	AGCM	–	1	5 years after 1 year spin-up

using the atmospheric part of MIROC5 was executed (aquaControl and aqua4xCO₂; APE hereafter). The aquaControl experiment adopts a zonally-uniform SST without sea ice at high latitude, following Neale and Hoskins (2000). The aqua4xCO₂ is identical to aquaControl, except that 4×CO₂ is imposed. For each run, 6-year integrations are performed, and climatologies in the latter 5 years analyzed. These 4×CO₂ sensitivity experiments were originally conceived as a part of CFMIP2 (Bony et al. 2011).

2.3 Transpose-AMIP II

In recent efforts toward better understanding of systematic errors in climate models, the weather forecast approach was proposed (Phillips et al. 2004; Williams and Brooks 2008). In this approach, climate models are run in “weather forecast mode”, with initial data from operational numerical weather prediction data or reanalyses. Development of forecast errors from all initialized states, averaged over cases, can provide insight into bias processes in the climatologies of long-term simulations (Rodwell and Palmer 2007). The new framework of the international model intercomparison project is referred to as the Transpose AMIP II (TAMIP hereafter; Xie et al. 2012; Williams et al. 2012). This approach can help discern what happens in climate models on fast timescales (e.g., clouds), and why responses differ at longer timescales. More details on TAMIP are available in Williams et al. (2012).

TAMIP data consist of a series of 10-day hindcasts initialized by European Center for Medium-Range Weather Forecasts (ECMWF) analysis for the year of tropical convection (YOTC; Waliser et al. 2012) period (May 2008 to April 2010). For this period, we conducted 4 sets (October 2008, January 2009, April 2009 and July 2009) of 16 hindcasts with the start times at 30 h intervals. In addition to the standard TAMIP experiments, we also did sensitivity tests with identical settings to the hindcasts but imposing quadrupled CO₂ in the atmosphere. Composite differences between 64 hindcasts and 4×CO₂ runs are calculated at every 3 h up to day 10. This ensures sampling throughout annual and diurnal cycles for a given lead time, which is expected to show how the transient adjustment to the abrupt 4×CO₂ evolves in time (S. Bony, personal communication).

2.4 Idealized experiments

To evaluate the role of land–sea thermal contrast in the tropospheric adjustment processes, we conducted idealized experiments with the APE as their basis. We set up five additional configurations: aqua-planet with different continent sizes (60°, 120°, 180°, 240°, and 300° longitudinal widths, hereafter L60, L120, L180, L240, L300,

respectively) in the tropics (30°S–30°N). The experiments with different sizes of continent could clarify whether effects of land–sea temperature contrast depend on continent size or not. Land elevation was uniformly set to 10 m, without mountains. Vegetation types were specified with zonally-uniform distribution, derived from the most prominent types at individual latitudes used in MIROC5. Similar to the APE, 6-year integrations were performed for control and sensitivity (4×CO₂) runs, with the latter 5 years analyzed in the individual configurations. Results are compared with those of the APE and AMIP in Sect. 4.

3 Tropospheric adjustment in cloud and hydrological cycle

3.1 Timescales of adjustment processes

First, we confirm the basic features of the radiative forcing and feedback in MIROC5 estimated using the regression method. Figure 1 shows the temporal evolution of global and annual-mean radiative fluxes at TOA versus SAT change in the single-member 4×CO₂ experiments. The effective radiative forcing due to 4×CO₂ estimated by the regression and fixed-SST methods are 8.9 and 8.7 W m⁻² respectively,

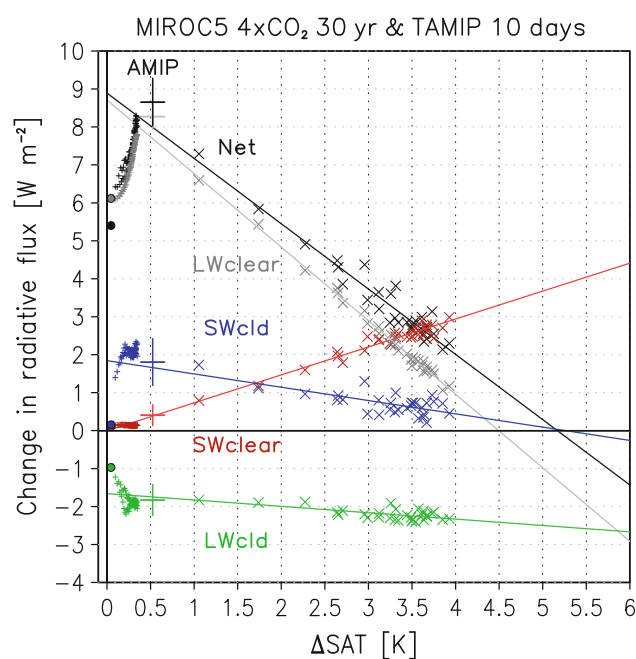


Fig. 1 Evolution of global mean radiative fluxes (W m⁻²) at TOA with global- and annual-mean SAT (K) in 4×CO₂ experiments using MIROC5 single-member AOGCM run over 30 years (‘X’ marks). Lines represent linear regression fits to annual-mean data. Small crosses represent 3-hourly data for 10 days from TAMIP experiment, averaged over 64 members. Circles represent 3-hourly means after CO₂ quadrupling. Large crosses represent equilibrium changes and ranges of standard deviations in AMIP 4×CO₂ experiment

which are slightly larger than the other CMIP5 models (Andrews et al. 2012a). The effective radiative forcing estimated here is consistent with that of Watanabe et al. (2010), but different from that of Andrews et al. (2012a) because the regression-based estimate depends on the analysis period (30 and 150 years in this study and Andrews et al. 2012a, respectively). The longwave (LW) components of clear-sky flux (LW_{clear}) and SW_{cl} forcings are positive (8.7 and 1.9 W m⁻², respectively), whereas the LW component of the CRE (LW_{cl}) forcing is negative (-1.7 W m⁻²). These values are almost identical to the equilibrium response to CO₂ quadrupling in the AMIP experiment (Fig. 1). The SW components of clear-sky flux (SW_{clear}) and LW_{clear} forcings have slightly different values between the fixed-SST (0.3 and 8.2 W m⁻²) and the regression methods (0.0 and 8.7 W m⁻²).

Also shown in Fig. 1 are high-frequency transient responses derived from the ensemble average of the TAMIP experiment. All the components reveal that the radiative forcing changes within the first 10 days with an ~0.3 K increase in SAT. During the first 3 h after atmospheric CO₂ quadrupling, SW_{clear} and SW_{cl} change little, but LW_{clear} and LW_{cl} show positive and negative changes, respectively. The transient change in LW_{clear} may be attributed to stratospheric adjustment and changes in tropospheric thermodynamic structure. The net radiation change largely follows the LW_{clear} change. The transient responses of SW_{cl} and LW_{cl} are presented in more detail in Fig. 2. In addition to the TAMIP and AMIP experiment results, the transient responses in daily data derived from the 12-member ensemble of the AOGCM 4×CO₂ experiment are plotted. The transient adjustments of SW_{cl} and LW_{cl} are very similar between TAMIP and AOGCM run in the first 1–2 days. This indicates that the adjustment of the CRE occurs similarly when SST can change because of the large thermal inertia of oceans. Further, daily-scale adjustments of the CRE from AOGCM run and TAMIP are comparable to those estimated in AMIP. Ocean- and land-mean adjustments to SW_{cl} and LW_{cl} have the same signs as those of the global mean although the former dominate the latter. These characteristics are robust across the experimental configurations, and the processes will be examined further below.

Changes in SAT, CRE, precipitation, and surface heat fluxes in the TAMIP 4×CO₂ experiments are shown in Fig. 3. In response to the abrupt CO₂ increase, all variables begin responding on a daily timescale. The increase of global mean SAT shows a gradual evolution on monthly and longer timescales, while the global mean CRE adjusts within 2 days (Fig. 3d–f). Precipitation decreases abruptly by -0.10 mm day⁻¹ and approaches the equilibrium response of -0.17 mm day⁻¹, which is well synchronized with a reduction of evaporation (Q_e; green curves in

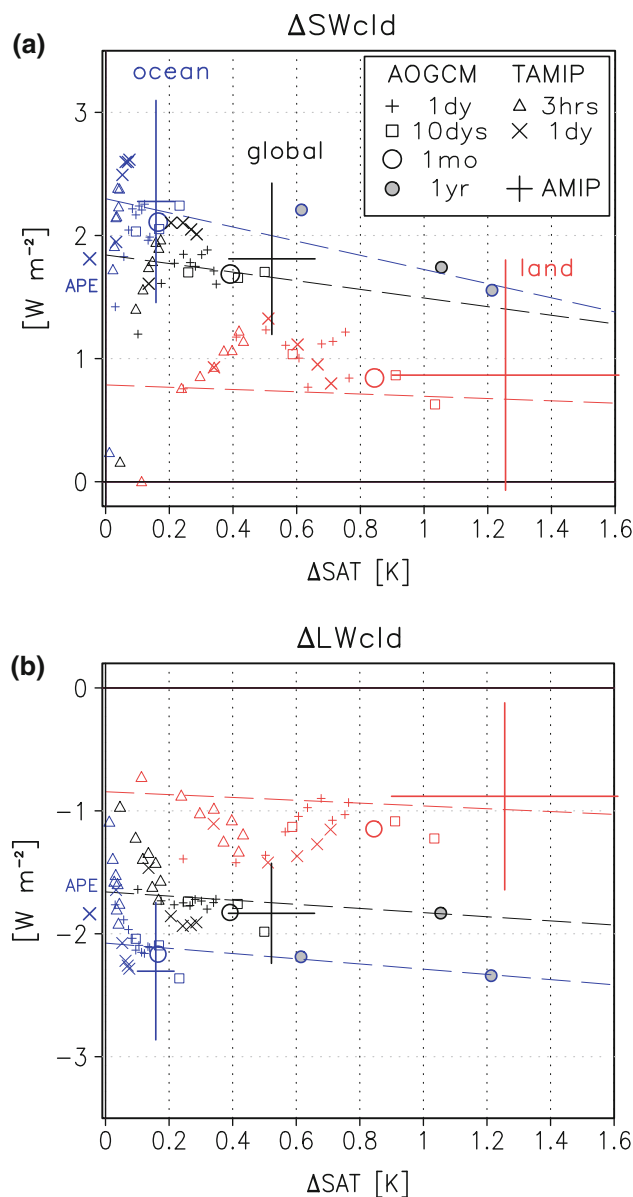


Fig. 2 Similar to Fig. 1 but for **a** SW_{cl} and **b** LW_{cl}. Black, red, and blue colors show global, land, and ocean means, respectively. 3-hourly and 1-daily data in TAMIP are drawn for the first 1 day and 5 days, respectively. Large crosses represent equilibrium changes and ranges of standard deviations in AMIP experiment. Data from 12-member ensemble of AOGCM experiments are overlaid (1-day, 10-day, 1-month, and 1-year means). Lines represent ordinary least squares regression fits to 30 years of annual-mean data in MIROC5 AOGCM (1 member). Crosses on left side represent equilibrium changes in aqua-planet experiment (APE)

Fig. 3g–i). These reductions indicate a slowdown of the hydrological cycle associated with tropospheric adjustment, as reported by Andrews et al. (2009). Sensible heat flux (Q_h) shows moderate change, because the change of difference between SAT and SST is small (Sect. 4). In contrast to changes over oceans, Q_h and Q_e on the land surface change instantaneously by approximately 0.12 and

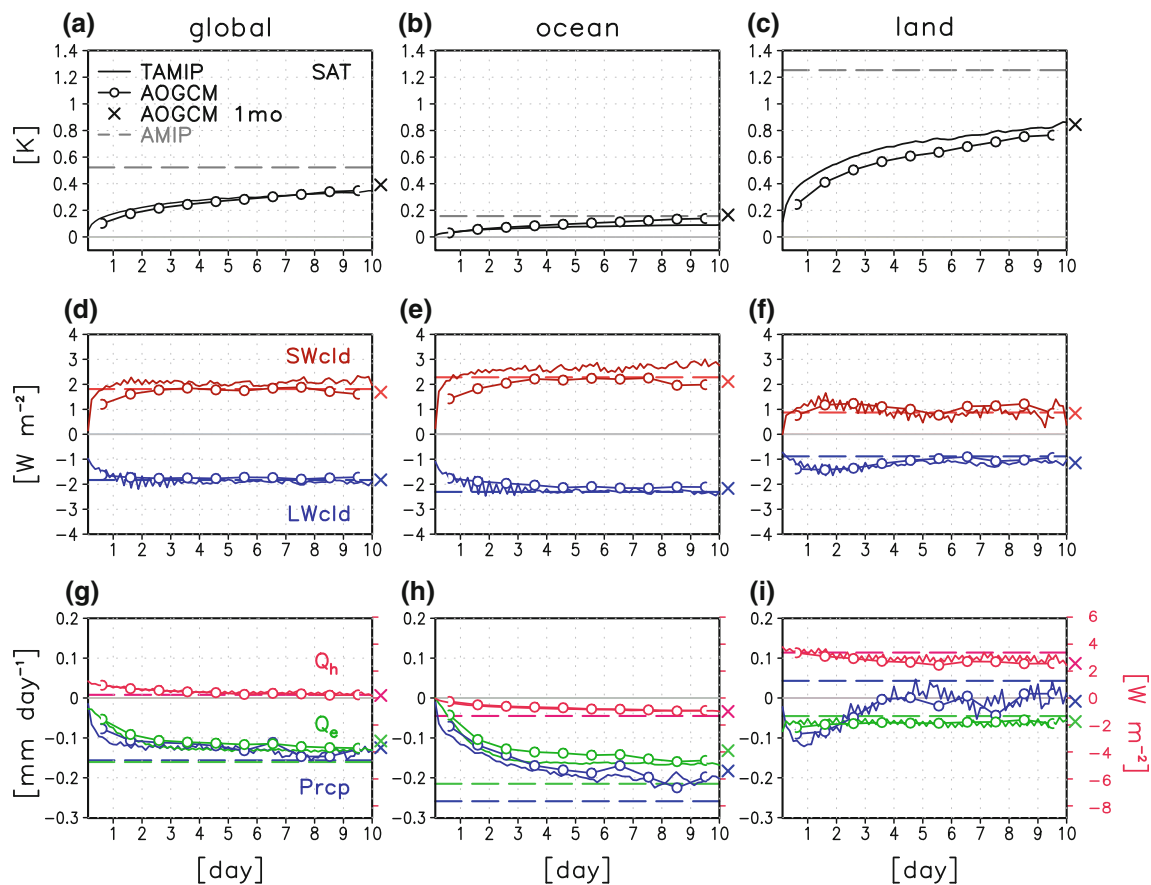


Fig. 3 Ensemble mean changes in **a** global mean SAT (K), **b** land-mean, and **c** ocean-mean in TAMIP $4\times\text{CO}_2$ experiments, relative to the control experiments. *Dashed lines* represent equilibrium changes in AMIP experiment. The *crosses* show the 1-month mean values in

the 12-ensemble means of AOGCM run. **d–f** SWcld and LWcld (W m^{-2}). **g–i** Q_h , Q_e (W m^{-2} , right axis) and precipitation (mm day^{-1} , left axis)

-0.06 W m^{-2} , respectively (Fig. 3i). These changes are consistent with what would be expected from changes in stomatal conductance (i.e. CO_2 physiological forcing, Doutriaux-Boucher et al. 2009; Andrews et al. 2011). The LWcld also has an instantaneous change (about -1.0 W m^{-2}) in the $4\times\text{CO}_2$ condition (Figs. 1, 2b, 3d), which is larger over the ocean (Fig. 3e). We term these time-invariant forcings, since they have no timescales and work to change other components immediately after CO_2 concentration is quadrupled. The negative time-invariant forcing in LWcld, which is larger over ocean than land, is consistent with the cloud masking effect (Soden et al. 2004; Andrews et al. 2012b; W12). Global mean values of cloud masking effects estimated by W12 are -1.1 and 0.1 W m^{-2} for LWcld and SWcld, consistent with the results shown in Figs. 1, 2b, and 3d–f. Cloud masking effects are generally comparable between GCMs that reproduce realistic cloud climatologies (W12). It therefore seems that the processes involved in tropospheric adjustment have at least three timescales: instantaneous, daily and slower adjustment.

3.2 Cloud adjustment

Given the daily adjustment of the CRE in MIROC5, we focused on changes in cloud and associated thermodynamic structure in the tropospheric adjustment process. We mainly show results over oceans, because the ocean mean adjustment dominates the global mean as illustrated in Sect. 3.1. Figure 4 shows a latitude-height section of transient and equilibrium changes in potential temperature (θ) over the oceans caused by CO_2 quadrupling. Evident in the equilibrium response is the stratospheric cooling and tropospheric warming with maxima in polar regions (Fig. 4d). In contrast to global warming experiments with increased SST (e.g. Lu et al. 2008), a peak warming in the tropical upper troposphere reflecting water vapor feedback does not emerge, because the fixed SST suppresses Q_e and precipitation rates (Fig. 3g). On a daily timescale, the lower troposphere warms first because of instantaneous LW radiative heating (e.g., Collins et al. 2006), with its peak at around 800–850 hPa (Fig. 4b, c). The warming then extends to

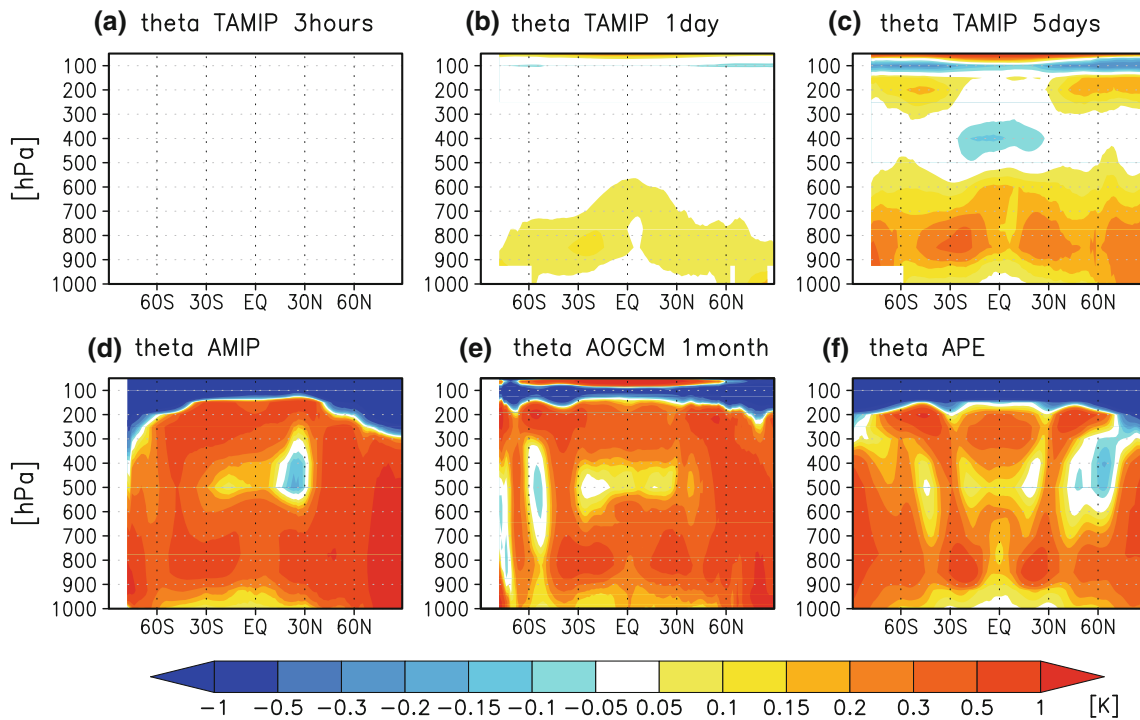


Fig. 4 Zonal mean changes in θ (K) over ocean in response to CO₂ quadrupling. **a** 3-h, **b** 1-day, and **c** 5-day means in TAMIP experiment. **d** Equilibrium changes in AMIP experiment. **e** 1-month mean in AOGCM run. **f** Same as **d**, but for APE

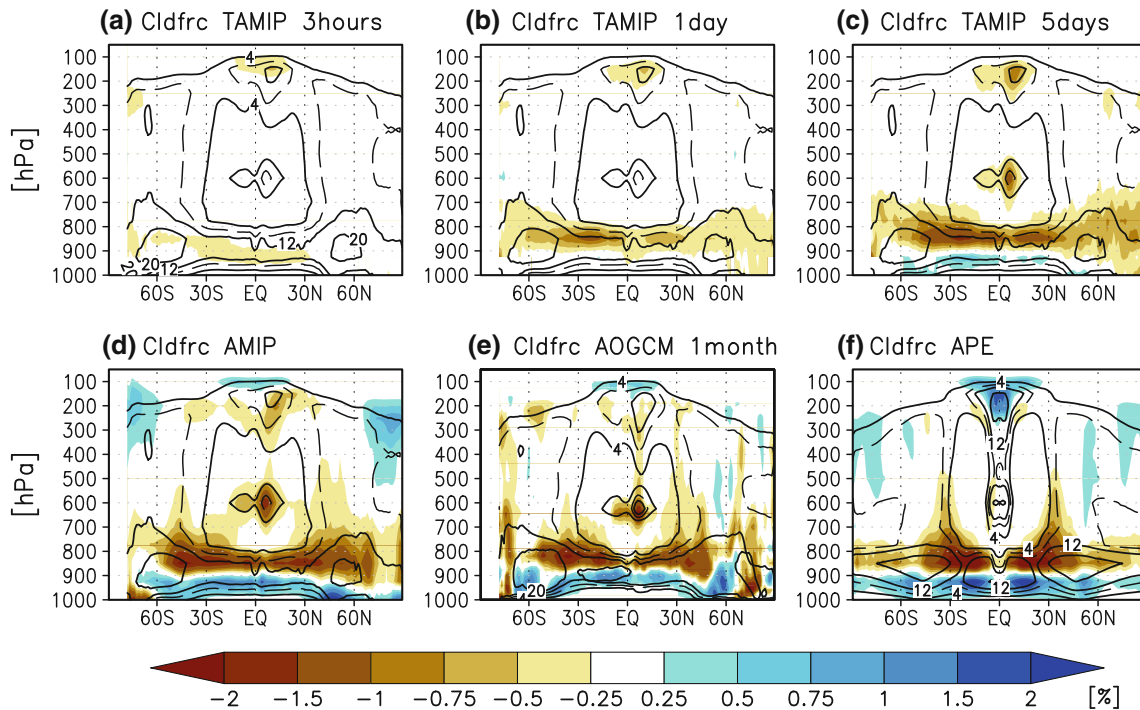


Fig. 5 Same as Fig. 4, but for cloud fraction (%). *Solid (dashed)* contours represent 4, 12, and 20 (8) % in control (amip, piControl, and aquaControl) simulations

700 hPa in transient (~ 0.2 K) and equilibrium (~ 0.4 K) responses, which increases vertical stability in the lower troposphere.

Figure 5 shows control values and changes of cloud fraction in various $4\times\text{CO}_2$ experiments. The climatological cloud amount in the control simulations (amip, piControl, aquaControl)

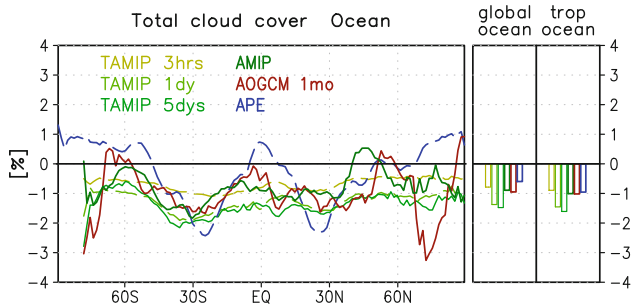


Fig. 6 Zonal mean changes in total cloud cover (%) over ocean. Bars on the right represent global- and tropical-mean (30°S to 30°N) values

and aquaControl) reveals a low cloud layer at 850–900 hPa. There are significant changes in the lower troposphere, namely: (1) reduction of cloud fraction; and (2) decreasing cloud height, which may be associated with the planetary boundary layer (PBL; detailed below). Figure 6 also shows changes in zonal-mean total cloud cover over the ocean. In the transient process and equilibrium responses in the tropospheric adjustment, a cloud cover decreases by 0.8–2.0 %, particularly in the subtropics. This indicates that the $4\times\text{CO}_2$ induces cloud decrease in the lower troposphere (Figs. 5, 6) and associated positive SWcld response in the tropospheric adjustment (Figs. 2a, 3e). Since the structure of low cloud changes is similarly identified in AOGCM and APE (Figs. 5e, f, 6), the two major changes in cloud adjustment as stated above are robust among the experimental configurations and less dependent upon the air–sea coupling and the land–sea contrast. Figure 7 shows changes in the vertical profiles of θ , cloud fraction, and relative humidity (RH). In response to the CO_2 increase, Q_e decreases (Fig. 3g–i) but temperature increases gradually, which reduces RH, particularly in the lower troposphere. The decreasing RH in the lower troposphere reduces the cloud fraction (Figs. 5, 6, 7c). At the 850 hPa level, a 1 % reduction in RH corresponds to ~ 0.6 % reduction in cloud fraction (Fig. 7c, e). In the middle and upper troposphere, cloud fraction shows a decreasing trend on daily timescale (150–400 hPa, Figs. 5a–d, 7c), which is consistent with the strengthening of negative LWcld change (Fig. 2b). Responses to the CO_2 increase over ocean and land show some differences. The tropospheric warming over land (Fig. 7b) precedes that over the ocean (Fig. 7a), owing to the fixed or small change in SST. Cloud fraction and RH near the surface (900–1,000 hPa) also show different characters between land and ocean. Over the ocean, near-surface RH increases (~ 0.5 %), but that over land decreases (approximately -1.2 %; Fig. 7e, f). The drying over land is consistent with the reduction of in situ Q_e (Fig. 3f) and a constraint of moisture transport from ocean associated with muted warming over ocean (e.g. Fasullo 2010). The slight

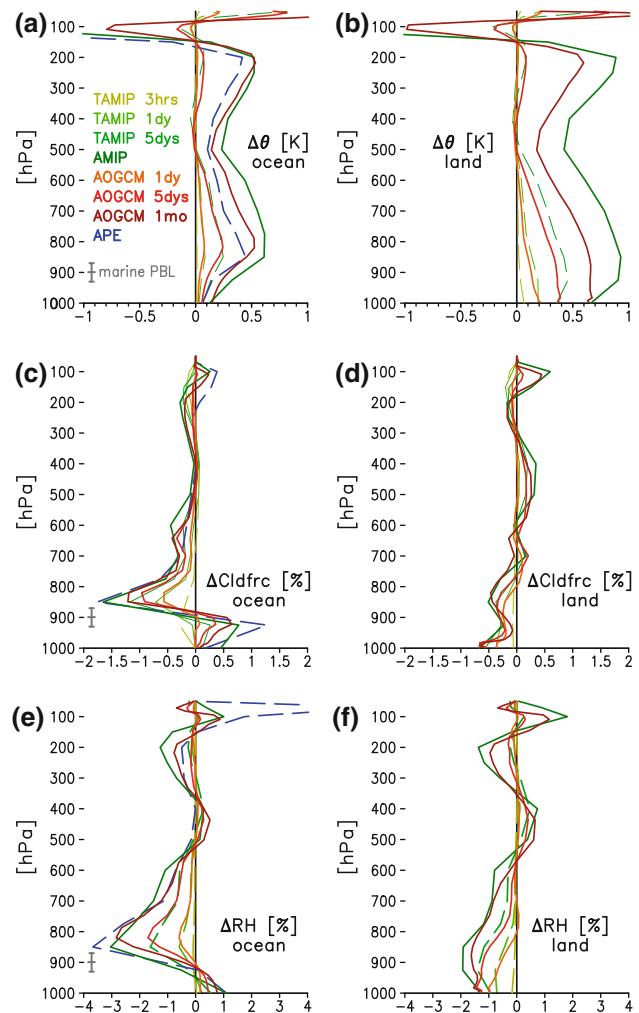


Fig. 7 Changes in θ (K) (a, b), cloud fraction (%) (c, d), and RH (%) (e, f) with height in $4\times\text{CO}_2$ experiments relative to control experiments over ocean (left) and land (right). Grey whiskers in a, c, e represents marine PBL depths and range of standard deviations

increase in near-surface RH over the ocean may be associated with weakening of vertical moisture transport in the lower troposphere (figures not shown) caused by increasing stability (Figs. 4, 7a). In response to the $4\times\text{CO}_2$, increase in stomatal resistance suppresses evapotranspiration and modifies the surface heat budget (decreasing Q_e and increasing Q_h ; Fig. 3i), then induces additional drying and warming over land (Fig. 7b, f).

The cloud fraction shows contrasting responses between 900–1,000 hPa (increase) and 800–900 hPa (decrease; Fig. 7c). Given that the height of climatological low cloud (850–900 hPa, Fig. 5) is controlled by PBL depth, the decreasing/increasing contrast is suggestive of PBL depth shoaling. Indeed, the spatial distribution of PBL depth diagnosed in the GCM shows shoaling in global oceans, except for polar regions (Fig. 8). The PBL depth rapidly declines 30–40 m in about 3 days, and continues to shoal

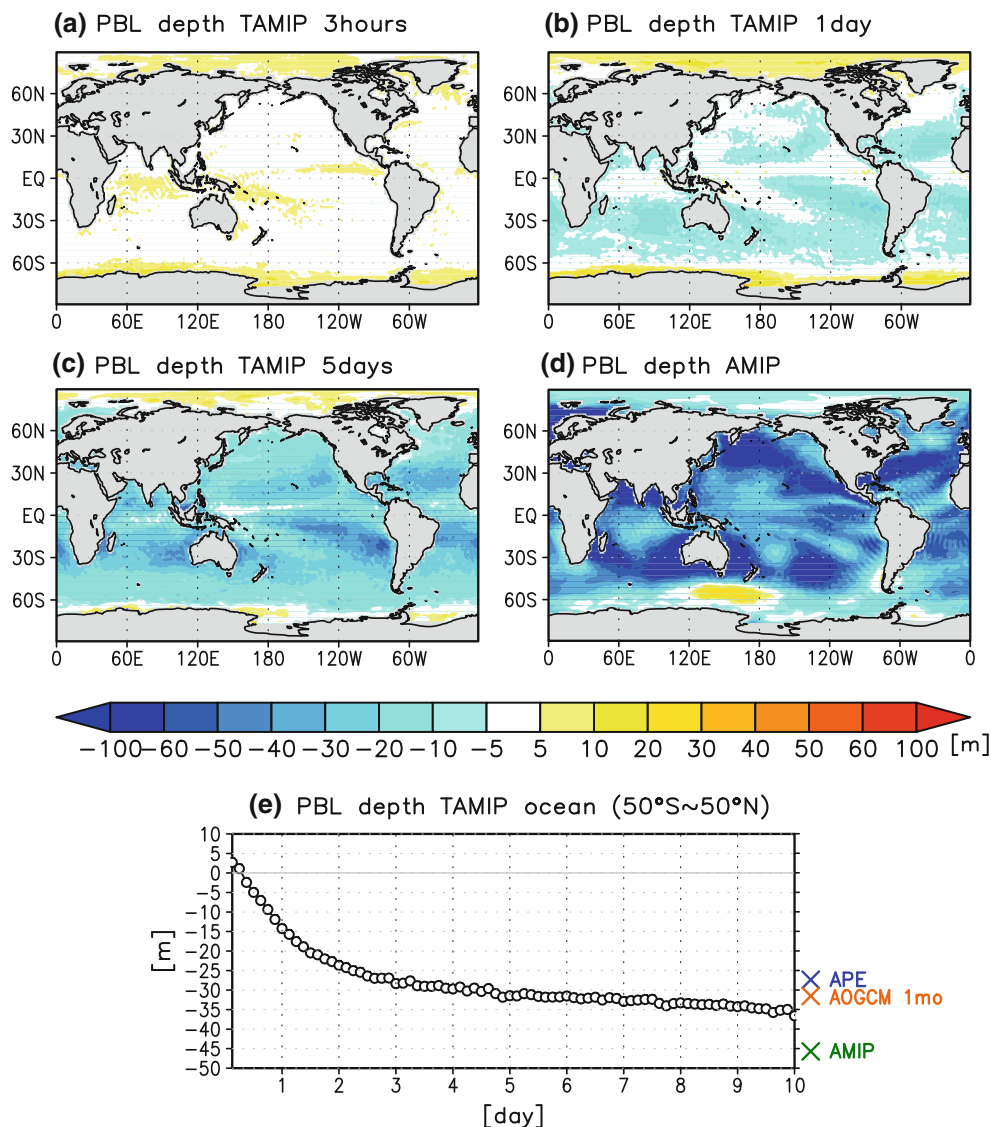


Fig. 8 Temporal evolution of marine PBL depth (m) anomalies in response to CO₂ quadrupling. **a** 3-h, **b** 1-day, and **c** 5-day means in TAMIP experiment. **d** Equilibrium changes in the AMIP experiment.

by day 10 in TAMIP (Fig. 8e). The PBL shoaling and general drying in the lower troposphere result in the strong decrease and weak increase of cloud at 800–900 hPa and 900–1,000 hPa, respectively. The response of PBL depth was also pointed out in previous studies (Watanabe et al. 2011; W12). In the next subsection, we examine possible mechanisms for the PBL shoaling associated with tropospheric adjustment.

3.3 Dynamic and thermodynamic changes and mechanisms for marine PBL shoaling

In addition to the changes in thermodynamic properties in the troposphere, the changes in the atmospheric dynamical

circulation may affect the cloud and associated SWcld perturbations in tropospheric adjustment over the ocean. To decompose dynamic and thermodynamic components of the SWcld responses over the tropics, we partition them into a series of dynamic regimes corresponding to different values of vertical pressure velocity (ω) at 500 hPa (ω_{500}). The change in SWcld in 4×CO₂ runs, Δ SWcld, is expressed following Bony et al. (2004):

circulation may affect the cloud and associated SWcld perturbations in tropospheric adjustment over the ocean. To decompose dynamic and thermodynamic components of the SWcld responses over the tropics, we partition them into a series of dynamic regimes corresponding to different values of vertical pressure velocity (ω) at 500 hPa (ω_{500}). The change in SWcld in 4×CO₂ runs, Δ SWcld, is expressed following Bony et al. (2004):

$$\Delta SWcld \approx \int_{\omega} SWcld_{\omega} \Delta P_{\omega} d\omega + \int_{\omega} P_{\omega} \Delta SWcld_{\omega} d\omega, \quad (1)$$

where P_{ω} represents the probability density function of ω_{500} , and $SWcld_{\omega}$ is a composite of SWcld with respect to ω_{500} in the control simulation. The first term is often called

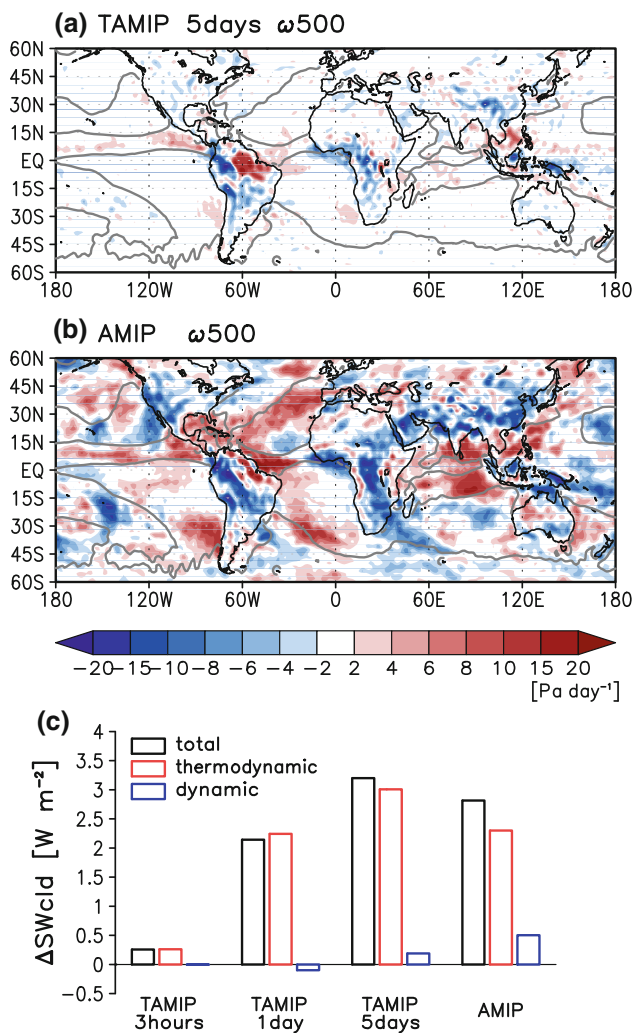


Fig. 9 **a** 5-day mean of change in ω_{500} (Pa day⁻¹) in TAMIP experiment, and **b** 30-year mean annual mean of change in AMIP experiment. Contours represent 0 hPa day⁻¹ in AMIP control simulation over ocean. **c** Decomposition of changes in tropical-mean (30°S to 30°N) SWcld (W m⁻²) over ocean (total, thermodynamic and dynamic components). The individual components in AMIP and TAMIP experiments are calculated by 30-year mean monthly mean data and 64-member ensemble 3-h, 1-day, and 5-day means data, respectively

the dynamic component, and the second term the thermodynamic component.

We first examine changes in the atmospheric circulation and contributions of the thermodynamic and dynamic terms to the positive SWcld response over the ocean in TAMIP and AMIP. Figure 9 shows changes in ω_{500} ($\Delta\omega_{500}$) during tropospheric adjustment on daily and longer timescales. In the equilibrium response (Fig. 9b), negative (positive) $\Delta\omega_{500}$ is generally confirmed over the ocean (land). As detailed in the next section, surface warming contrast evolves rapidly between land and ocean and then induces anomalous downward (upward) motion

over the ocean (land) in the adjustment process. The positive $\Delta\omega_{500}$ over the ocean mainly appears in convective regimes (e.g. Inter-Tropical Convergence Zones in the Indian Ocean, western North Pacific, eastern North Pacific, and equatorial western Atlantic). Some regions in the subtropics show negative $\Delta\omega_{500}$, indicating weakening of large-scale atmospheric circulation. The general weakening of atmospheric circulation with tropospheric adjustment has been documented in previous studies (LWJ11; W12). However, changes in atmospheric circulation are very slight on a daily timescale (3-h and 1-day means, not shown). By day 5, the negative $\Delta\omega_{500}$ over land and weakening of upward motion in the ascent regime partially appears, but a slowdown of the entire atmospheric circulation is not clear over the ocean (Fig. 9a). Figure 9c shows contributions of the dynamic and thermodynamic components to the SWcld perturbation in TAMIP and AMIP in the tropics (30°S–30°N). The positive SWcld evolving within 2 days (Fig. 3e) is mainly attributable to the thermodynamic component (Fig. 9c), indicating that the dynamic component contributes little to perturbations in the CRE on a daily timescale. In the equilibrium response, the contribution of the dynamic component attributed to the weakening atmospheric circulation over the ocean is about 18 %, which is not negligibly small.

Next we focus on the thermodynamic changes that regulate the CRE response in tropospheric adjustment evolving within 2 days. Figure 10 shows changes in cloud fraction and CRE sorted by ω_{500} in the control simulation. Decreasing low cloud ($\eta \sim 0.85$) is prominent in the subsidence regime. Clouds in the mid- and upper troposphere in convective (i.e., ascent) regimes decrease in the transient and equilibrium responses. Corresponding to the evolution of the cloud adjustment, ocean-mean values of the CRE adjust in 2 days, when SWcld shows a positive adjustment (~ 3 W m⁻²) associated with the decrease of low cloud. The increasing SWcld is larger in the subsidence regime than the convective regime (Fig. 9e–h). The adjustment in LWcld has a larger negative value in the convective regime (about -3 W m⁻²) than the subsidence regime (about -2 W m⁻²) due to decreases of mid and high clouds in the convective regime. As represented in Figs. 1, 2, 3, LWcld has a negative value as a time-invariant forcing, particularly in the ascent regime.

In the tropospheric adjustment in MIROC5, a shoaling of the marine PBL is a common feature among experimental configurations. In this subsection, we examine relationships between changes in PBL depth and other variables to discover possible mechanisms for the PBL shoaling. Figure 11 shows transient and equilibrium responses of PBL depth and other variables sorted by ω_{500} . As shown in Figs. 8 and 10, the PBL shoaling is greater in the subsidence regime than the convective regime

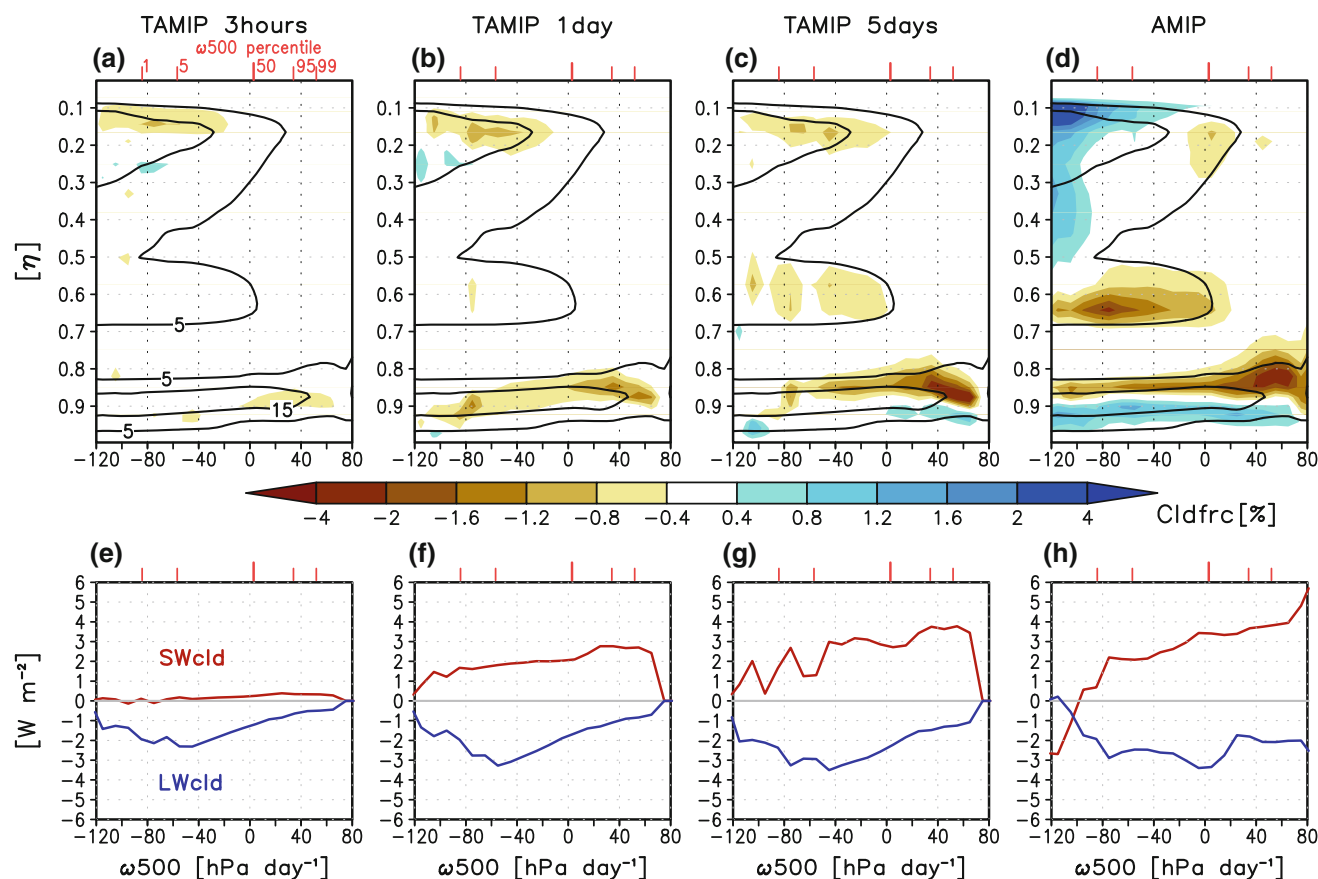


Fig. 10 Regime composite of changes in **a–d** cloud fraction (%) and **e–h** CRE (SWcld and LWcld, W m^{-2}) over ocean with respect to vertical pressure velocity at 500 hPa (ω_{500}). Red ticks on the x-axis represent percentiles of ω_{500} . **a, e** 3-h, **b, f** 1-day, and **c, g** 5-day

(Fig. 11e–h). The PBL shoals gradually on both daily and longer timescales. The shoaling of the marine PBL in the strong subsidence region (50–60 m) is comparable to those in W12 (63–114 m). The spatial and temporal features of the PBL shoaling are consistent with changes in Q_h and Q_e (Fig. 11e–h). Changes in SAT and surface RH shown in Fig. 11a–d reveal gradual increases in the subsidence regime (0.05 K and 0.5 %, respectively). Because of the fixed-SST condition, increases in SAT and surface RH suppress Q_h and Q_e from the sea surface. Change in surface wind speed is also a regulating factor for surface heat flux changes, but is of secondary importance (figures not shown). Reduction of buoyancy production owing to suppressed surface heat fluxes (-4 to -8 W m^{-2} in Q_e and 0.05 – 0.10 W m^{-2} in Q_h) is important for the PBL shoaling (Watanabe et al. 2011).

In addition to the suppression of surface heat fluxes, the change in vertical stability is a control on PBL depth (Medeiros et al. 2005). Figure 12 shows changes in θ and LW radiative heating rate in individual circulation regimes. As shown in other studies (Collins et al. 2006; Colman and

McAvaney 2011), the instantaneous LW heating rate caused by the CO₂ increase peaks in the lower troposphere ($\eta = 0.8$ – 0.9 ; Fig. 12e). This is part of the time-invariant forcing that drives the rapid adjustment processes. Because of the instantaneous LW heating (Fig. 12e–h), the lower troposphere warms up gradually on daily and longer timescales (Fig. 12a–d). The warming is predominant in the free troposphere ($\eta < 0.85$), but greatly restricted in the PBL and near the surface because of the surface constraint (i.e., fixed SST). The profile of temperature change is a robust feature among models (Dong et al. 2009; Colman and McAvaney 2011; W12). The contrasting change of temperature between the free troposphere and PBL strengthens vertical stability and thereby suppresses vertical turbulent mixing that otherwise maintains a thick PBL.

4 Role of land–sea contrast in tropospheric adjustment

So far, we have focused on the adjustment processes over oceans, because they are the major factors for global mean

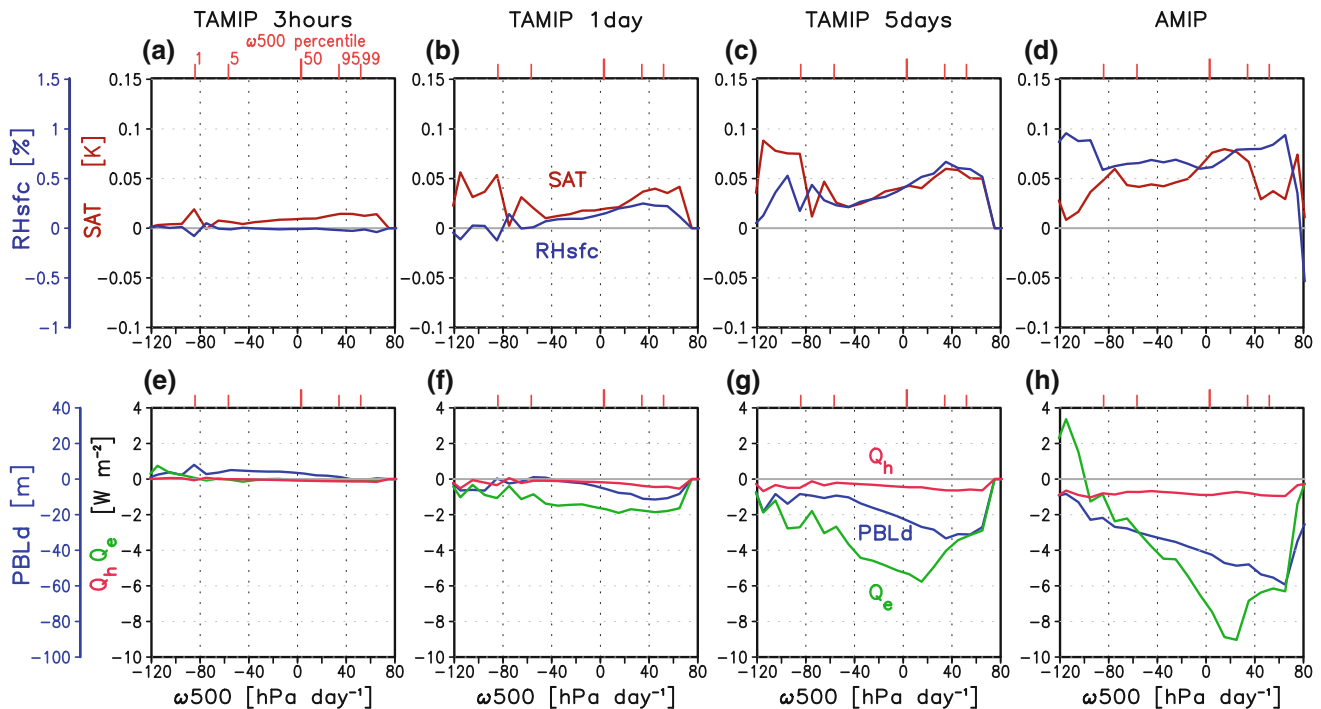


Fig. 11 Same as Fig. 10e–h but for SAT (K) and surface RH (%) (a–d), Q_h and Q_e ($W m^{-2}$) and PBL depth in m (e–h)

adjustment in the CRE (Figs. 2, 3). However, the responses of dynamical motion, cloud, and CRE show clear contrasts between land and ocean (Figs. 3, 7, 9), indicating the significant contribution of the land–sea warming contrast to the tropospheric adjustment. In this section, we examine whether cloud and CRE changes associated with that contrast are essential for tropospheric adjustment, using idealized experiments. Figure 13 shows changes in SAT and SWcld due to CO_2 quadrupling in the APE, AMIP, and idealized experiments. Because of the fixed SST, SAT changes little over the ocean (Fig. 13a) but increases significantly (1–3 K) over land (Fig. 13b–d), generating the surface warming contrast between land and ocean. As shown in Figs. 1, 2, 3, global mean and ocean-mean responses in SWcld (LWcld) to $4\times CO_2$ are positive (negative) in MIROC5. The positive change in SWcld peaks in the subtropics ($\sim 2 W m^{-2}$; Figs. 6, 13e). Figure 14 shows changes in cloud amount in response to the CO_2 increase. The positive SWcld response in the subtropics corresponds to decreasing cloud amount, particularly in the lower troposphere (Figs. 5, 6, 9, 14e). High cloud in the subtropics shows less change than low cloud (Fig. 14a). LWcld shows a negative adjustment in AMIP and APE (Fig. 2b), without substantial change in high cloud amount (Fig. 14a, c), suggesting the cloud masking effect.

With the existence of a continent at low latitude, increasing SAT over land (Fig. 13b) generates anomalous upward motion in the troposphere (figures not shown); this

increases deep convective cloud over land (Fig. 14b). The change in high cloud is greater than for mid-low clouds (Fig. 14f), leading to an increase in total cloud cover and associated negative SWcld response over the continent (Fig. 13f). These changes are consistent with those reported in the previous studies (LWJ11, W12) and are roughly opposite to the cloud adjustment over the ocean (decreasing high cloud and a positive SWcld response; Figs. 13b, d, 14b, d). It indicates that the ocean and land have positive and negative contributions to the global mean cloud adjustment, respectively. Patterns of changes in high cloud and SWcld in the AMIP experiment (Figs. 13g, 14c) do show some similarities to the idealized experiments, and are perhaps generated partly by a circulation change associated with equatorial waves (Matsuno 1966; Gill 1980). The land surface warming at low latitudes enhances convective heating, which forces a dynamical Matsuno-Gill response. Decreasing high cloud over the western coast of the continent (Fig. 14b, d) is collocated with a pair of cyclonic circulation changes straddling the equator, which resembles the Matsuno-Gill pattern (figure not shown). The above feature is also found in the AMIP experiment with some modification, because of meridional asymmetry in the land–sea contrast (Figs. 13g, 14c).

As land size increases, the area of increasing SAT and cloud cover and associated negative SWcld response becomes wider horizontally (Figs. 13b, d, f, h, 14b, d, f, h). Because of the wave-like responses of the circulation and cloud to the CO_2 increase, complex patterns appear over land

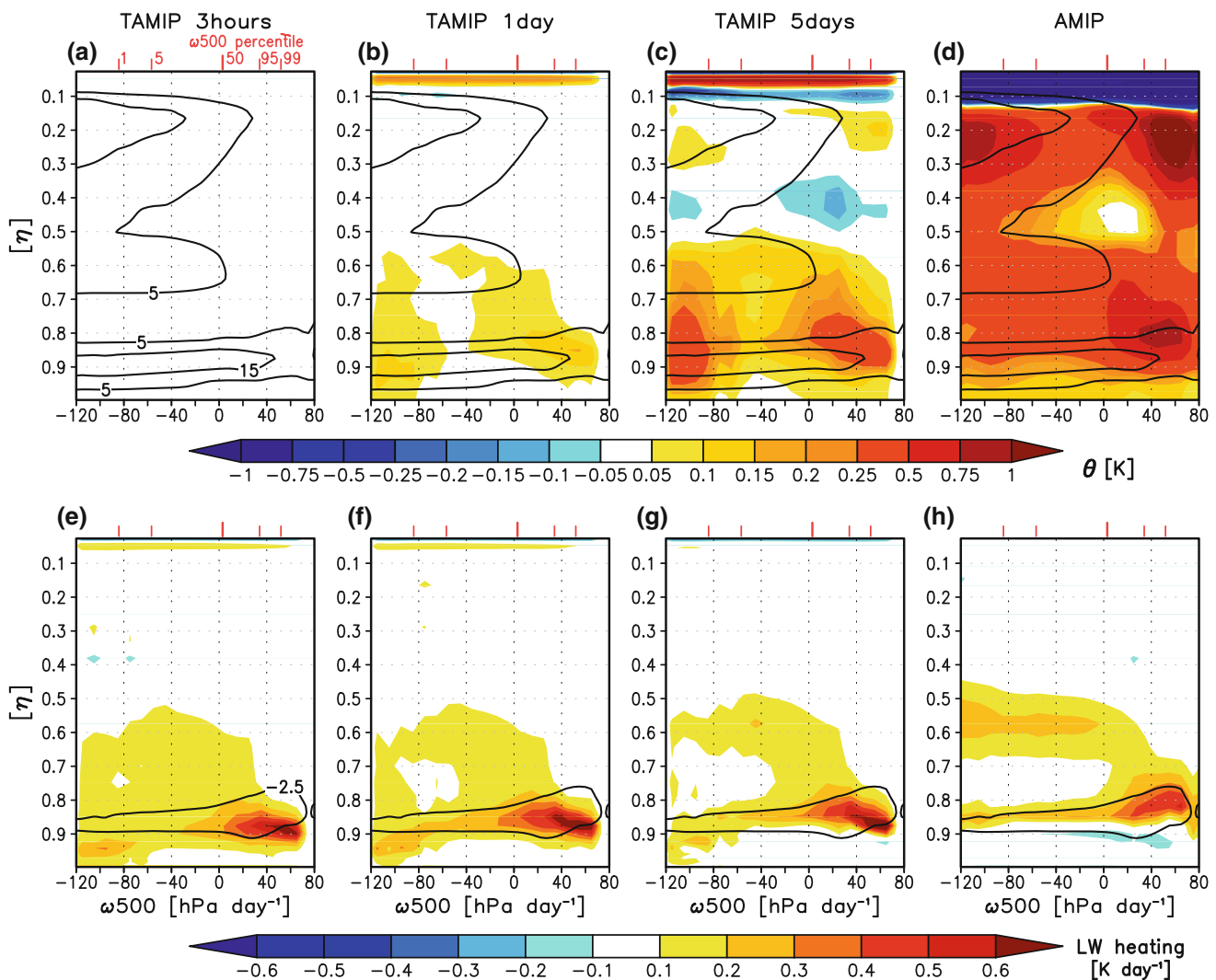


Fig. 12 Same as Fig. 10a–d but for θ (K) (a–d), and LW heating rate (K day^{-1}) (e–h). Contours in a–d and e–h are climatology of cloud fraction (%) and LW heating rate (K day^{-1}) in AMIP control simulation, respectively

and ocean in both idealized and AMIP experiments. Although it is difficult to decompose land and ocean contributions to these complex changes, we identified a systematic difference among six idealized models when tropical-mean changes in SAT, SWcld, and LWcld were calculated (Fig. 15). The fractional coverage of land at low latitude is about 25 % in the AMIP experiment, and is therefore plotted between L60 and L120. The response in SAT shows strong dependency on land size (Figs. 13a–d, 15a). SWcld and LWcld also change with increasing land size. As the land becomes larger, its effect on tropical-mean cloud and CRE adjustments becomes more prominent (Fig. 15b, c). This relationship indicates that land size is a regulating factor of the tropospheric adjustment. However, the land can weaken the total adjustment but cannot change its sign. This suggests that the land–sea warming contrast is a secondary factor and not essential for the cloud

adjustment processes, consistent with the results shown in Sect. 3.2.

5 Concluding discussions

The transient processes on different timescales (i.e., instantaneous, daily, and slower) in tropospheric adjustment to increasing CO₂ were explored using MIROC5, under the CMIP5/CFMIP2 framework and idealized experimental settings. The transient evolution of the tropospheric adjustment was detected well by the 64-member ensemble following the TAMIP sensitivity tests. The processes of tropospheric adjustment over the ocean are summarized in Fig. 16. Instantaneous radiative forcing from the 4×CO₂ warms the mid-lower troposphere, which

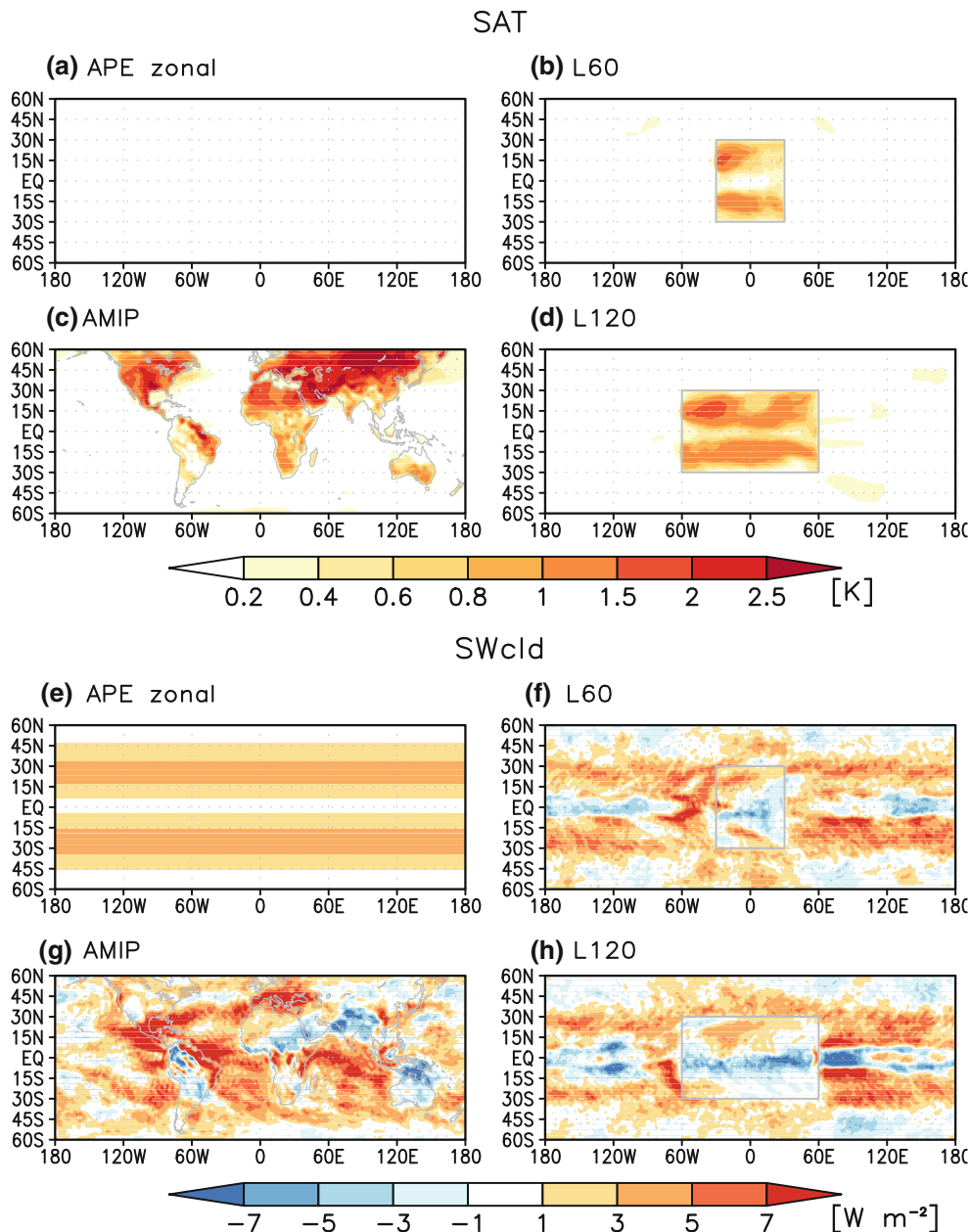


Fig. 13 Changes in SAT (K) (a–d), and SWcld (W m^{-2}) (e–h) in response to CO_2 quadrupling in AMIP, APE, and rectangular continent experiments. APE (zonal-mean) (a, e), L60 (b, f), AMIP (c, g), and L120 (d, h). Grey lines represent land shapes in individual experiments

strengthens vertical stability in the lower troposphere. For the fast timescale that does not allow SST to respond, increases in SAT and surface RH suppress sensible and latent heat fluxes (Q_h and Q_e) from the sea surface. The warming but suppressed Q_e results in the lower tropospheric drying, which acts to reduce clouds. At the same time, suppressed buoyancy production from the sea surface and strengthened vertical stability reduce marine PBL depth. These effects decrease and increase clouds in the lower troposphere and near the surface respectively, in which the cloud decrease dominates and thereby SWcld

change should be positive. All these processes are sufficiently rapid, reaching equilibrium within 2 days. Changes in atmospheric circulation make a minor contribution to tropospheric adjustment on a daily timescale.

The analyses based on different timescales indicate that the conventional concept of effective radiative forcing can be largely decomposed into three parts: (1) time-invariant forcing (instantaneous radiative forcing, CO_2 physiological forcing, and cloud masking effect); (2) adjustment on a daily timescale (rapid responses to the instantaneous radiative forcing, i.e., stratospheric adjustment, surface

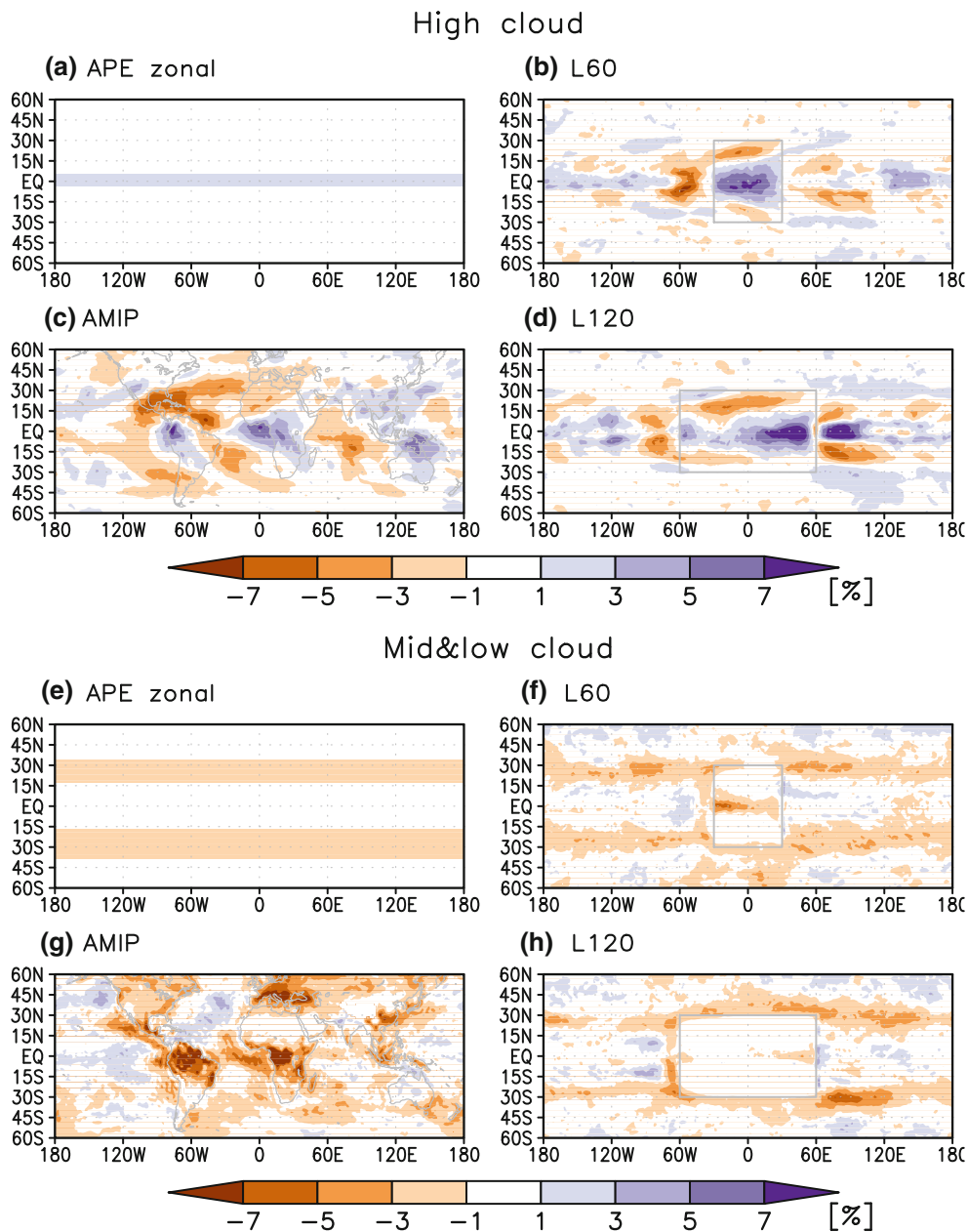


Fig. 14 Same as Fig. 13, but for high level cloud (a–d) and mid- and low-level cloud (%) (e–h)

warming and anomalous upward motion over land, warming, drying, and cloud decrease in lower troposphere and associated CRE response, strengthened vertical stability in the lower troposphere, suppressed surface heat fluxes and hydrological cycle, and PBL shoaling); and (3) slower adjustment (additional changes in tropospheric temperature, surface heat fluxes, PBL depth, and strength of large-scale atmospheric circulation). The responses of tropospheric temperature, surface heat fluxes, and PBL depth are initially rapid and continue on slower timescales.

The land–sea warming contrast modifies the large-scale atmospheric circulation and cloud amount, which affect the

tropospheric adjustment. Anomalous upward motion induced by land surface warming results in increasing high cloud and an associated negative change in SWcld over land, which partially compensates for the positive change in SWcld over the ocean. The effect of the land surface warming depends on continental size, indicating that land size is a regulating factor for tropospheric adjustment in this model. The land warming negatively contributes to the global mean tropospheric cloud adjustment, but the land effect cannot change the sign of the total adjustment. It is suggested that the land–sea warming contrast is just a secondary factor for the tropospheric adjustment.

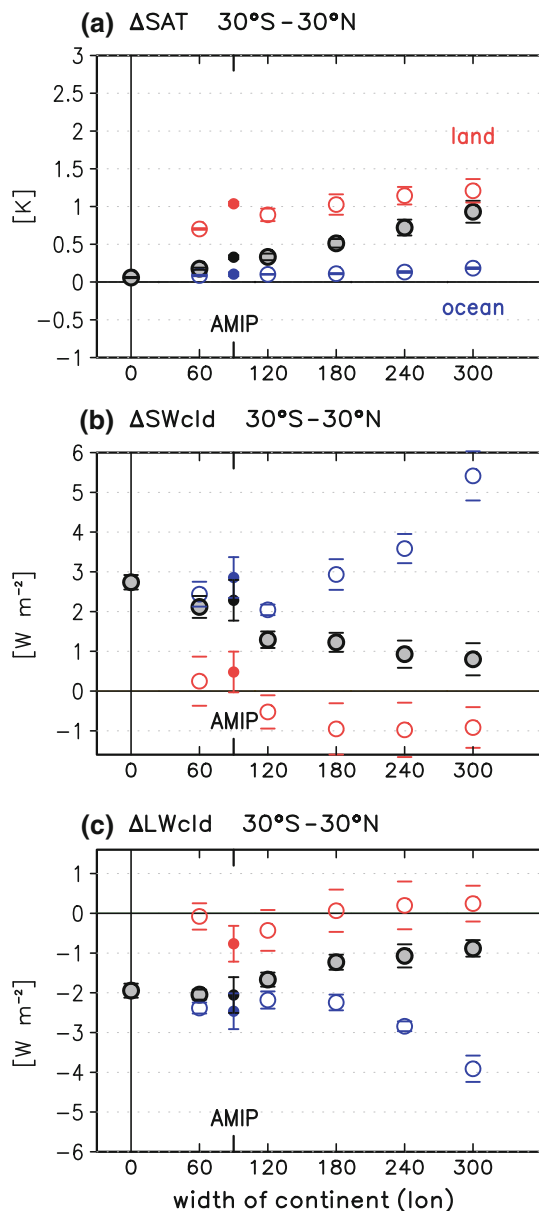


Fig. 15 Changes of SAT (K) (a), SWcld (b), and LWcld (W m^{-2}) (c), averaged over the tropics (30°S – 30°N) in APE, AMIP, and rectangular continent experiments. Black, red, and blue colors represent tropics, tropical land, and tropical ocean averages. Ranges of standard deviation are also plotted

This is the first application of the TAMIP $4\times\text{CO}_2$ experiments to detect the fast response to instantaneous radiative forcing. Most parts of the effective radiative forcing and tropospheric adjustments detected by the TAMIP ensemble are consistent with equilibrium response in the AMIP (fixed SST) $4\times\text{CO}_2$ experiment, but they have some discrepancies relative to those estimated by the regression method in the AOGCM $4\times\text{CO}_2$ experiment. GW08 compared geographic distributions of tropospheric adjustment estimated by the two methods and revealed

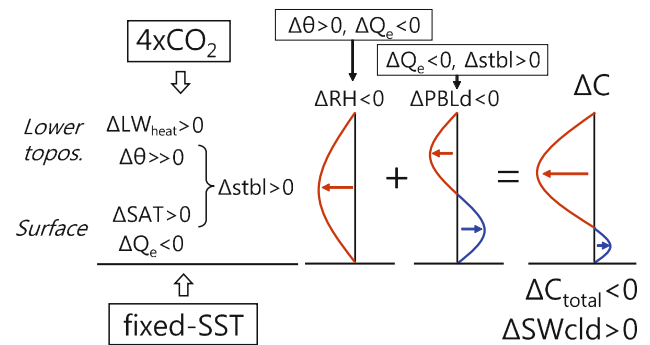


Fig. 16 Schematic of the physical processes of the cloud and SWcld in tropospheric adjustment in the lower troposphere and near-surface over the ocean. $\Delta\text{LW}_{\text{heat}}$, Δstbl , and ΔPBLd represent changes in LW radiative heating rate, atmospheric vertical stability, and depth of PBL, respectively. ΔC and $\Delta\text{C}_{\text{total}}$ represent changes in cloud fraction and total cloud fraction, respectively. Red (blue) lines represent decreasing (increasing) C

some differences, particularly in the tropics. Andrews et al. (2012a) applied the regression and fixed-SST methods to the CMIP5 multi-models, revealing differences mainly due to non-linear responses of TOA radiative budget to global-mean SAT increase over long-term integrations (150 years). They showed that, in some models, effective radiative forcing estimated by the fixed-SST method and change of TOA net radiation in the first year tend to fall above the regression line. They also stated that the largest contributor to the non-linear response is SWcld over the ocean. The non-linear response may exist on decadal and longer timescales, which may be related to delayed sea surface warming, stratocumulus response, and state of the deep ocean (Andrews et al. 2012a). The TAMIP experiment would aid quantitative evaluation of estimated effective radiative forcings among different methods and timescales.

The changes in cloud and stratification associated with tropospheric adjustment shown here are generally consistent with previous studies on the tropospheric adjustment (e.g. Dong et al. 2009; Colman and McAvaney 2011). WLG12 reported that the majority of CMIP3/CFMIP1 models show positive (negative) changes in SWcld (LWcld) and strengthening of vertical tropospheric stability with tropospheric adjustment. In contrast, W12 revealed slight increases in tropical- and global-mean total cloud fractions together with the shoaling of the marine PBL. Different responses of high-, mid- and low-level cloud, and associated CRE from those in other models would be related to differences in the model physical schemes (cloud, shallow cumulus, turbulence, and radiation) and configurations (e.g. GCMs, cloud resolving GCMs). The MIROC5 model used in this study reproduces cloud and water vapor generally well but underestimates high cloud relative to the other CMIP5 models (Jiang et al. 2012). The

reproducibility of cloud in the control simulation might be a factor for the tropospheric cloud adjustment to increasing CO₂. The finding in this study is based only on a particular CMIP5 model, which should therefore be validated using multi-models under the CFMIP2/CMIP5 umbrella. In particular, changes in atmospheric thermodynamic structure (temperature and humidity), surface heat fluxes, PBL depth, large-scale atmospheric circulations and cloud amounts could be key ingredients for the inter-model spread of Δ SW_{wld}. For detection of evolution processes in response to external forcings, other applications of the TAMIP ensemble (e.g., solar constant, aerosols, patterned-SST anomaly) may also be worth developing. Such approaches may facilitate other groups to interpret evolution processes and possible mechanisms for inter-model spread within forcing and feedback studies.

Acknowledgments We would like to acknowledge Hideo Shiogama, Tomoo Ogura, Tokuta Yokohata and Seita Emori at the National Institute for Environmental Studies (NIES), Masakazu Yoshimori and Rei Nobui at the Atmosphere and Ocean Research Institute (AORI), University of Tokyo, and Manabu Abe at the National Institute of Polar Research (NIPR) for providing helpful comments and suggestions. The authors are grateful to two anonymous reviewers for their constructive comments. This work was supported by the Program for Risk Information on Climate Change (PRICC) and Grants-in-Aid 23310014 and 23340137 from the Ministry of Education, Culture, Sports, Science and Technology (MEXT), Japan.

Open Access This article is distributed under the terms of the Creative Commons Attribution License which permits any use, distribution, and reproduction in any medium, provided the original author(s) and the source are credited.

References

- Allen MR, Ingram WJ (2002) Constraints on future changes in climate and the hydrologic cycle. *Nature* 419:224–232
- Andrews T, Forster PM (2008) CO₂ forcing induces semi-direct effects with consequences for climate feedback interpretations. *Geophys Res Lett* 35:L04802. doi:10.1029/2007GL032273
- Andrews T, Forster PM, Gregory JM (2009) A surface energy perspective on climate change. *J Clim* 22:2557–2570
- Andrews T, Forster PM, Boucher O, Bellouin N, Jones A (2010) Precipitation, radiative forcing and global temperature change. *Geophys Res Lett* 27:L14701. doi:10.1029/2010GL043991
- Andrews T, Doutriaux-Boucher M, Boucher O, Forster PM (2011) A regional and global analysis of carbon dioxide physiological forcing and its impact on climate. *Clim Dyn* 36:783–792
- Andrews T, Gregory JM, Webb MJ, Taylor KE (2012a) Forcing, feedbacks and climate sensitivity in CMIP5 coupled atmosphere-ocean climate models. *Geophys Res Lett* 39:L09712. doi:10.1029/2012GL051607
- Andrews T, Gregory JM, Forster PM, Webb MJ (2012b) Cloud adjustment and its role in CO₂ radiative forcing and climate sensitivity: a review. *Surv Geophys* 33:619–635
- Bala G, Caldeira K, Nemani R (2010) Fast versus slow response in climate change: implications for the global hydrological cycle. *Clim Dyn* 35:423–434
- Boer GJ (2011) The ratio of land to ocean temperature change under global warming. *Clim Dyn* 37:2253–2270
- Bony S, Dufresne J-L, LeTreut H, Morcrette J-J, Senior C (2004) On dynamic and thermodynamic components of cloud changes. *Clim Dyn* 22:71–86
- Bony S, Webb MJ, Bretherton CS, Klein SA, Siebesma AP, Tselioudis G, Zhang M (2011) CFMIP: towards a better evaluation and understanding of clouds and cloud feedbacks in CMIP5 models. *CLIVAR Exch* 16(56):20–24
- Boucher O, Jones A, Betts RA (2009) Climate response to the physiological impact of carbon dioxide on plants in the Met Office Unified Model HadCM3. *Clim Dyn* 32:237–249
- Cess RD et al (1990) Intercomparison and interpretation of climate feedback processes in 19 atmospheric general circulation models. *J Geophys Res* 95:16601–16615
- Collins WD et al (2006) Radiative forcing by well-mixed greenhouse gases: estimates from climate models in the Intergovernmental Panel on Climate Change (IPCC) fourth assessment report (AR4). *J Geophys Res* 111:D14317. doi:10.1029/2005JD006713
- Colman RA, McAvaney BJ (2011) On tropospheric adjustment to forcing and climate feedbacks. *Clim Dyn* 36:1649–1658
- Dommenget D (2009) The ocean's role in continental climate variability and change. *J Clim* 22:4939–4952
- Dong B, Gregory JM, Sutton RT (2009) Understanding land-sea warming contrast in response to increasing greenhouse gases. Part I: transient adjustment. *J Clim* 22:3079–3097
- Doutriaux-Boucher M, Webb MJ, Gregory JM, Boucher O (2009) Carbon dioxide induced stomatal closure increases radiative forcing via a rapid reduction in low cloud. *Geophys Res Lett* 36:L02703. doi:10.1029/2008GL036273
- Fasullo JT (2010) Robust land-ocean contrasts in energy and water cycle feedback. *J Clim* 23:4677–4693
- Gill AE (1980) Some simple resolutions for heat-induced tropical circulation. *Q J R Meteor Soc* 106:447–462
- Good P, Gregory JM, Lowe JA (2011) A step-response simple climate model to reconstruct and interpret AOGCM projections. *Geophys Res Lett* 38:L01703. doi:10.1029/2010GL045208
- Gregory JM, Webb MJ (2008) Tropospheric adjustment induces a cloud component in CO₂ forcing. *J Clim* 21:58–71
- Gregory JM, Ingram WJ, Palmer MA, Jones GS, Stott PA, Thorpe RB, Lowe JA, Johns TC, Williams KD (2004) A new method for diagnosing radiative forcing and climate sensitivity. *Geophys Res Lett* 31:L03205. doi:10.1029/2003gl018747
- Hansen J et al (2002) Climate forcings in Goddard Institute for Space Studies S12000 simulations. *J Geophys Res* 107. doi:10.1029/2001JD001143
- Hansen J et al (2005) Efficacy of climate forcings. *J Geophys Res* 110:D18104. doi:10.1029/2005JD005776
- Hasumi H, Emori S (2004) K-1 coupled model (MIROC) description. K-1 technical report. Center for Climate System Research, University of Tokyo, 34 pp. Available at <http://www.ccsr.u-tokyo.ac.jp/kyosei/hasumi/MIROC/tech-repo.pdf>
- Jiang JH et al (2012) Evaluation of cloud and water vapor simulations in CMIP5 climate models using NASA “A-Train” satellite observations. *J Geophys Res* 117:D14105. doi:10.1029/2011JD017237
- Knutti R, Hegerl GC (2008) The equilibrium sensitivity of the earth's temperature to radiation changes. *Nat Geosci* 1:735–743
- Lambert FH, Webb MJ (2008) Dependency of global mean precipitation on surface temperature. *Geophys Res Lett* 35:L16706. doi:10.1029/2008GL034838
- Lambert FH, Webb MJ, Joshi MM (2011) The relationship between land-ocean surface temperature contrast and radiative forcing. *J Clim* 24:3239–3256
- Lu J, Chen G, Frierson DMW (2008) Response of the zonal mean atmospheric circulation to El Niño versus global warming. *J Clim* 21:5835–5851

- Manabe S, Spelman MJ, Stouffer RJ (1991) Transient responses of a coupled ocean–atmosphere model to gradual changes of atmospheric CO₂. Part I: annual mean response. *J Clim* 4:785–818
- Matsuno T (1966) Quasi-geostrophic motions in equatorial areas. *J Meteorol Soc Jpn* 44:25–43
- Medeiros B, Hall A, Stevens B (2005) What controls the mean depth of the PBL? *J Clim* 18:3157–3172
- Mitchell JFB, Wilson CA, Cunningham WM (1987) On CO₂ climate sensitivity and model dependence of results. *Q J R Meteorol Soc* 113:293–322
- Neale R, Hoskins B (2000) A standard test for agcms including their physical parametrizations I: the proposal. *Atmos Sci Lett* 1:101–107
- Phillips TJ, Potter GL, Williamson DL, Cederwall RT, Boyle JS, Fiorino M, Hnilo JJ, Olson JG, Xie S, Yio JJ (2004) Evaluating parameterizations in general circulation models: climate simulation meets weather prediction. *Bull Am Meteor Soc* 85:1903–1915
- Rodwell MJ, Palmer TN (2007) Using numerical weather prediction to assess climate models. *Q J R Meteorol Soc* 133:129–146
- Sellers PJ, Bounoua L, Collatz GJ, Randall DA, Dazlich DA, Los SO, Berry JA, Fung I, Tucker CJ, Field CB, Jensen TG (1996) Comparison of radiative and physiological effect of doubled atmospheric CO₂ on climate. *Science* 271:1402–1406
- Shiogama H, Watanabe M, Yoshimori M, Yokohata T, Ogura T, Annan JD, Hargreaves JC, Abe M, Kamae Y, O’ishi R, Nobui R, Emori S, Nozawa T, Abe-Ouchi A, Kimoto M (2012) Perturbed physics ensemble using the MIROC5 coupled atmosphere-ocean GCM without flux corrections: experimental design and results. *Clim Dyn*. doi:10.1007/s00382-012-1441-x
- Soden BJ, Broccoli AJ, Hemler RS (2004) On the use of cloud forcing to estimate cloud feedback. *J Clim* 17:3661–3665
- Sutton RT, Dong B, Gregory JM (2007) Land/sea warming ratio in response to climate change: IPCC AR4 model results and comparison with observations. *Geophys Res Lett* 34:L02701. doi:10.1029/2006GL028164
- Taylor KE, Stouffer RJ, Meehl GA (2012) An overview of CMIP5 and the experiment design. *Bull Am Meteorol Soc* 90:485–498
- Waliser DE et al (2012) The “year” of tropical convection (May 2008 to April 2010): climate variability and weather highlights. *Bull Am Meteorol Soc* 93:1189–1218. doi:10.1175/2011BAMS3095.1
- Watanabe M, Suzuki T, O’ishi R, Komuro Y, Watanabe S, Emori S, Takemura T, Chikira M, Ogura T, Sekiguchi M, Takata K, Yamazaki D, Yokohata T, Nozawa T, Hasumi H, Tatebe H, Kimoto M (2010) Improved climate simulation by MIROC5: mean states, variability, and climate sensitivity. *J Clim* 23:6312–6335
- Watanabe M, Shiogama H, Yoshimori M, Ogura T, Yokohata T, Okamoto H, Emori S, Kimoto M (2011) Fast and slow timescales in the tropical low-cloud response to increasing CO₂ in two climate models. *Clim Dyn*. doi:10.1007/s00382-011-1178-y
- Watanabe M, Shiogama H, Yokohata T, Kamae Y, Yoshimori M, Ogura T, Annan JD, Hargreaves JC, Emori S, Kimoto M (2012) Using a multi-physics ensemble for exploring diversity in cloud-shortwave feedback in GCMs. *J Clim* 25:5416–5431
- Webb MJ, Lambert FH, Gregory JM (2012) Origins of differences in climate sensitivity, forcing and feedback in climate models. *Clim Dyn*. doi:10.1007/s00382-012-1336-x
- Williams KD, Brooks ME (2008) Initial tendencies of cloud regimes in the Met Office Unified Model. *J Clim* 21:833–840
- Williams KD, Bodas-Salcedo A, Deque M, Fergin S, Medeiros B, Watanabe M, Jakob C, Klein SA, Senior CA, Williamson DL (2012) The Transpose-AMIP II experiment and its application to the understanding of Southern Ocean cloud biases in climate models. *J Clim* (submitted)
- Wu Y, Seager R, Ting M, Naik N, Shaw TA (2012) Atmospheric circulation response to an instantaneous doubling of carbon dioxide. Part I: model experiments and transient thermal response in the troposphere. *J Clim* 25:2862–2879
- Wyant MC, Bretherton CS, Blossey PN, Khairoutdinov M (2012) Fast cloud adjustment to increasing CO₂ in a super parameterized climate model. *J Adv Model Earth Syst* 4:M05001. doi:10.1029/2011MS000092
- Xie S, Ma H-Y, Boyle JS, Klein SA, Zhang Y (2012) On the correspondence between short- and long- timescale systematic errors in CAM4/CAM5 for the years of tropical convection. *J Clim*. doi:10.1175/JCLI-D-12-00134.1